

Tidal Dissipation in Evolved Low and Intermediate Mass Stars

M. Esseldeurs¹, S. Mathis², and L. Decin¹

¹ Instituut voor Sterrenkunde, KU Leuven, Celestijnenlaan 200D, 3001 Leuven, Belgium
 e-mail: mats.esseldeurs@kuleuven.be

² Université Paris-Saclay, Université Paris Cité, CEA, CNRS, AIM, 91191 Gif-sur-Yvette, France

Received; accepted

ABSTRACT

Context. Context

Aims. Aims

Methods. Methods

Results. Results

Conclusions. Conclusion

Key words. key1 — key2 — key3

1. Introduction

Tidal interactions have long been recognised as a fundamental factor influencing the evolution of stellar and planetary systems. In particular, the dissipation of tidal forces plays a crucial role in shaping the structural and dynamical characteristics of stars, with significant implications for their overall evolutionary trajectory. While tidal effects have been studied extensively in various contexts, our focus in this investigation is on the tidal dissipation strengths of stars throughout their entire lifetime, with a particular emphasis on the evolved phases.

Tidal dissipation is a complex process characterized by two components: equilibrium and dynamical tides. The former arises from the hydrostatic displacement induced by the ellipsoidal deformation triggered by a stellar companion. The energy associated with the equilibrium tide is dissipated through turbulent friction in convective layers, leading to the transfer of angular momentum between the stellar spin and its orbital motion. This well-established mechanism has been studied in various contexts, including investigations of asymptotic giant branch (AGB) stars (Mustill & Villaver 2012; Madappatt et al. 2016). In contrast to the equilibrium tide, the dynamical tide involves the excitation of stellar oscillation modes by the tidal potential. This dynamical tide has yet to be formally evaluated systematically in the evolved phases, despite its crucial role for subgiants and red giant branch (RGB) stars (Weinberg et al. 2017; Ahuir et al. 2021).

In this study, we bridge this gap by conducting a comprehensive investigation into the equilibrium and dynamical tides during the evolved phases. Utilising established theoretical frameworks and stellar evolution simulations, we aim to quantify and compare the strengths of these two tidal components, providing a complete understanding of their contributions to the overall dissipation of tidal energy all along the stars lifetime.

Add more observations. Not sure which references?

2. Tidal dissipation modelling

In this section, we provide a brief overview of the theoretical frameworks used to model the equilibrium and dynamical tides.

2.1. General framework

Considering two bodies, for instance a star and a planet, where we only consider the deformation of one object, in this case the star. The gravitational potential of the secondary object (the planet) can be expressed as a multipole expansion in spherical harmonics. The tidal potential is then given by the difference between the gravitational potential of the secondary object and the gravitational potential of a point mass located at the center of the primary object (the star). The tidal potential can be expressed as (Ogilvie 2014)

$$\Psi = \text{Re} \left\{ \sum_{l=2}^{\infty} \sum_{m=0}^l \sum_{n=-\infty}^{\infty} \frac{Gm_p}{a} A_{l,m,n}(e, i) \left(\frac{r}{a} \right)^l Y_l^m(\theta, \phi) e^{-in\Omega_o t} \right\} \quad (1)$$

where m_p is the mass of the companion object, a is the semi-major axis of the orbit, e is the eccentricity of the orbit, i is the inclination of the orbit, r, θ, ϕ are spherical coordinates in the primary object, Y_l^m are the spherical harmonics, $\Omega_o = \sqrt{GM_\odot/a^3}$ is the mean motion, and $A_{l,m,n}$ are the tidal coefficients (see Ogilvie 2014 table 1). In this study we focus on a coplanar circular orbit. In this case only the $l = m = n = 2$ terms are non-zero in the quadrupolar approximation ($l > 2$ is neglected), and the tidal potential can be expressed as

$$\Psi = \text{Re} \left\{ \frac{Gm_p}{a} \sqrt{\frac{6\pi}{5}} \left(\frac{r}{a} \right)^2 Y_2^2(\theta, \phi) e^{-in\Omega_o t} \right\} = \left\{ \varphi_T Y_2^2(\theta, \phi) e^{-in\Omega_o t} \right\} \quad (2)$$

Since $Y_2^2 \propto e^{im\phi}$, the tidal potential has a complex argument $m\phi - n\Omega_o t$. This means that the tidal potential rotates with a frequency $\omega_t = n\Omega_o - m\Omega_s$, where ω_t is the tidal frequency and

Ω_s is the spin frequency of the star. This frequency will be the characteristic frequency of the tidal waves excited in the star.

Tidal dissipation can be expressed in multiple formalisms, using for instance the tidal quality factor Q , the modified tidal quality factor Q' or the love number k_l^m . The tidal quality factor is defined as the ratio between the energy stored in the tidal bulge and the energy dissipated per orbit. The Love number is the ratio between the perturbation of the gravitational potential induced by the presence of the planetary companion and the tidal potential, evaluated at the stellar surface. The tidal quality factor and the Love number are related by

$$Q_l^m(\omega_t)^{-1} = \text{sgn}(\omega_t) |k_l^m(\omega_t)|^{-1} \text{Im} [k_l^m(\omega_t)] = \sin [2\delta_l^m(\omega_t)] \quad (3)$$

and the modified tidal quality factor is related to the tidal quality factor and the Love number by

$$\text{Im} [k_l^m(\omega_t)] = \omega_t \frac{3}{2Q_l^m(\omega_t)} = \omega_t \frac{k_l^m}{Q_l^m} \quad (4)$$

2.2. Tidal wave excitation

In order to understand the tidal dissipation in the star, it is important to understand what types of waves can be excited in the star, and more importantly what types of waves can be excited by the tidal potential. The tidal potential is a periodic potential, and therefore it can only excite waves with a frequency equal to the tidal frequency ω_t , the frequency at which the tidal potential rotates. If it is possible to excite waves at these frequencies, the excitation of these waves will lead to additional dissipation of energy and angular momentum, called the dynamical tide. In this subsection the different types of waves that can be excited in the star are discussed, assuming a companion on a circular orbit at a distance of 1 AU.

2.2.1. Inertial waves

Inertial waves are waves that have the Coriolis force as a restoring force. These waves can only be excited in rotating stars, and only for sufficiently low frequencies in the regime $\omega \in [-2\Omega, 2\Omega]$. For tides to excite inertial waves, their frequency needs to be in this regime, and therefore $\Omega_o < 2\Omega_s$. This means that for sufficiently slow rotating stars, the tidal potential cannot excite inertial waves.

Stars with a convective envelope during the Main Sequence (MS) phase are spun down during this phase because of magnetic braking, and therefore if there is no sufficiently massive companion to spin up the star, the tidal potential cannot excite inertial waves during its subsequent evolution. Stars without a convective envelope during the MS don't experience this spin down, and are expected to still have significant rotation rates during their subsequent evolution. However observations of these stars still show low rotation rates during the RGB (Ceillier et al. 2017), either due to stronger rotational damping than predicted by models, or due to differential rotation within the star. Rotation during the AGB phase has been investigated theoretically including only the equilibrium tide, where rotation rates found in these studies predict sufficient spin up (but still low rotation rates) to excite inertial waves for stellar mass companions (García-Segura et al. 2016; Madappatt et al. 2016), but not enough for Jupyter mass companions, or absence of a companion (García-Segura et al. 2014; Madappatt et al. 2016).

Depending on the internal structure of the star, different types of inertial waves can be excited. When the star is fully convective, global normal modes can be excited (Wu 2005a,b), while

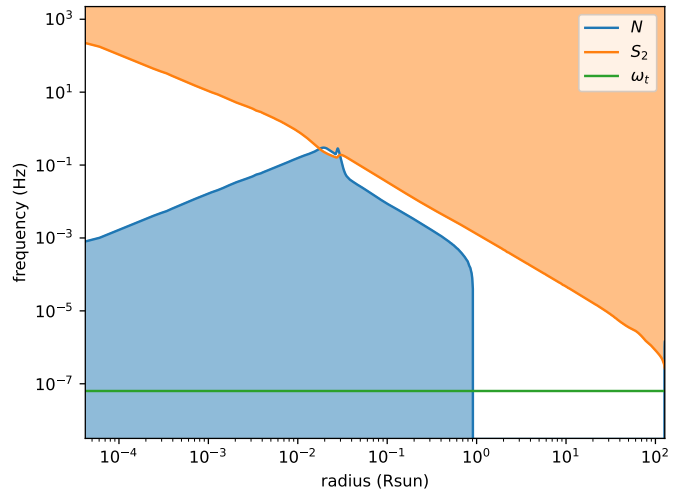


Fig. 1. Brunt-Väisälä, Lamb and tidal frequency.

when the star has a radiative interior, wave attractors can be excited due to the reflection of the waves at the boundaries of the radiative zone (Ogilvie 2013). The strength of the excitation of these waves depends on the Ekman number $\text{Ek} = v_t/(2\Omega R_\star^2)$, with v_t the turbulent viscosity. For low Ekman numbers, the excitation of these waves is strong, while for high Ekman numbers, the excitation of these waves is suppressed (Auclair Desrotour et al. 2015). For evolved stars, the Ekman number (typically on the order of 10^{-1}) is sufficiently high to suppress the excitation of these waves, and therefore the excitation of these waves is not considered in this study.

2.2.2. Pressure waves

Pressure waves (p-waves) are waves that have the pressure as a restoring force. These waves can be excited at frequencies higher than the Lamb-frequency $S_l = \frac{l(l+1)c_s^2}{r^2}$ with c_s the local sound speed. The Lamb-frequency for $l = 2$ as a function of radius is shown in Fig. 1 for a star with initial mass of $1 M_\odot$ during the AGB phase. Here the tidal frequency is also shown for a planet on a circular orbit at a distance of 1 AU. As can be seen, the tidal frequency is always lower than the Lamb-frequency, and therefore no pressure waves can always be excited by the tidal potential.

2.2.3. Gravity waves

Gravity waves (g-waves) are waves that have buoyancy as a restoring force. These waves can be excited at frequencies lower than the Brunt-Väisälä frequency $N^2 = g_0 \left(\frac{\partial_r \rho_0}{\Gamma_1 \rho_0} - \frac{\partial_r \rho_0}{\rho_0} \right)$. This Brunt-Väisälä frequency as a function of radius is shown in Fig. 1 for a star with initial mass of $1 M_\odot$ during the AGB phase. Here the tidal frequency is also shown for a planet on a circular orbit at a distance of 1 AU. As can be seen, the tidal frequency is much lower than the maximal Brunt-Väisälä frequency ($\omega_t \ll N_{\max}$), and therefore gravity waves in the form of internal gravity waves (IGW) can be excited by the tidal potential, and need to be taken into account when computing the dynamical tide.

Depending on how efficient the radiative damping is in damping these g-waves, the waves are either damped before they

can be reflected at the boundaries of the radiative zone, or they are reflected at the boundaries and travel back and forth through the radiative zone. The former is what type of waves are called progressive gravity waves, while in the latter case, the reflecting interaction of the waves can create gravity modes. The two cases are separated by the critical frequency ω_c , which is the frequency at which the radiative damping is strong enough to damp the waves with a factor e before they can be reflected at the boundaries of the radiative zone. The critical frequency can be expressed as (Alvan et al. 2015):

$$\omega_c = [l(l+1)]^{\frac{3}{8}} \left(\left| \int_{r_{\text{in}}}^{r_{\text{out}}} K_T \frac{N^3}{r_1^3} dr_1 \right| \right)^{\frac{1}{4}} \quad (5)$$

where K_T is the thermal diffusivity. Frequencies lower than the critical frequency are progressive gravity waves, while frequencies higher than the critical frequency are gravity modes.

Here r_{in} and r_{out} are the inner and outer boundaries of the radiative zone assuming a three-layered structure (see Fig. 2). In the case there is only a convective core and a radiative envelope, $r_{\text{in}} = 0$ and $r_{\text{out}} = r_c$. In the case there is a convective core, a radiative envelope, and a convective envelope, $r_{\text{in}} = r_c$ and $r_{\text{out}} = R_{\star}$. In the case of a true 3-layered structure, one needs to be careful with this definition as waves starting at the inner boundary may interact with waves starting at the outer boundary, and still create g-modes while being in the progressive wave regime.

The critical frequency in evolved stars is higher than the tidal frequency (see e.g. Fig. 8), and therefore the tidal potential can only excite progressive gravity waves.

2.3. Tidal dissipation

2.3.1. Equilibrium tide

The equilibrium tide is the tidal dissipation originating from the hydrostatic deformation of an object due to the gravitational potential of a companion. The equilibrium tide is dissipated through turbulent friction in convective layers, leading to the transfer of angular momentum between the stellar spin and its orbital motion. In order to calculate the dissipation of the equilibrium tide, the tidal displacement of the star needs to be calculated. This displacement can be calculated by first calculating the non-wavelike component of the gravitational potential Φ_l^{nw} which can be calculated using the differential equation (Dhouib et al. 2023):

$$\frac{1}{r^2} \frac{d}{dr} \left(r^2 \frac{d\Phi_l^{nw}}{dr} \right) - \frac{l(l+1)}{r^2} \Phi_l^{nw} + 4\pi G \rho_0 \frac{d\rho_0}{dP_0} (\Phi_l^{nw} + \Psi_l) = 0 \quad (6)$$

with ρ_0 the density, P_0 the pressure, and Ψ_l the tidal potential. Boundary conditions are chosen to ensure regularity at the center, and continuity at the surface (Dhouib et al. 2023):

$$\begin{cases} \frac{d \ln \Phi_l^{nw}}{d \ln r} = l & \text{at } r = \eta R_{\star} \text{ for } \eta \rightarrow 0 \\ \frac{d \ln \Phi_l^{nw}}{d \ln r} = -(l+1) & \text{at } r = R_{\star} \end{cases} \quad (7)$$

When the non-wavelike component of the gravitational potential is known, the tidal displacement can be calculated as (Dhouib et al. 2023):

$$\xi_{r,l}^{nw} = -\frac{\Phi_l^{nw} + \Psi_l}{g_0}, \quad \xi_{h,l} = \frac{1}{l(l+1)} \left(2\xi_{r,l}^{nw} + r \frac{d\xi_{r,l}^{nw}}{dr} \right). \quad (8)$$

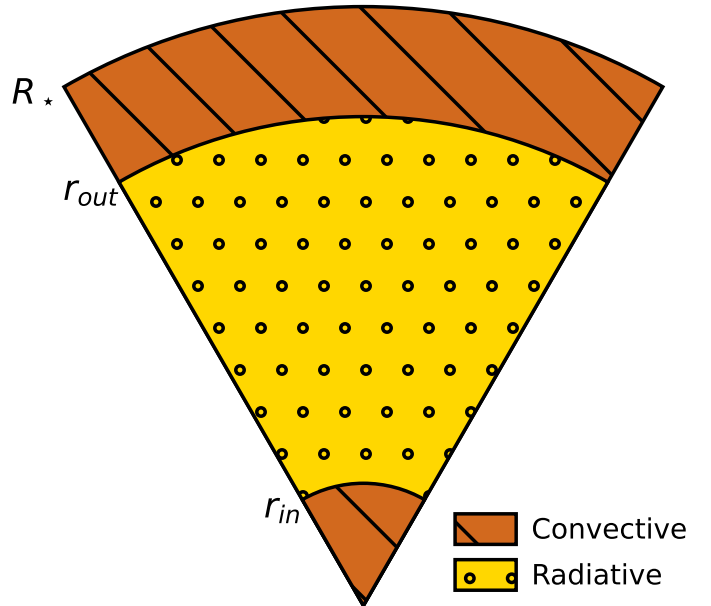


Fig. 2. Schematic representation of the 2 and 3 layered structure of the star.

where this displacement can be used to calculate the dissipation of the equilibrium tide (Barker 2020):

$$[\text{Im } k_2^2]_{eq} = \frac{16\pi G \omega_t^2}{4(2l+1)R_{\star}^{2l+1}|A|^2} \int_0^{R_{\star}} r^2 \nu_t D_l(r) dr, \quad (9)$$

with

$$D_l(r) = \left(3 \frac{d\xi_{r,l}^{nw}}{dr} - \frac{1}{r^2} \frac{d(r^2 \xi_{r,l}^{nw})}{dr} + l(l+1) \frac{\xi_{h,l}^{nw}}{r} \right)^2 + l(l+1) \left(\frac{\xi_{r,l}^{nw}}{r} + r \frac{d(\xi_{h,l}^{nw}/r)}{dr} \right)^2 + (l-1)l(l+1)(l+2) \left(\frac{\xi_{h,l}^{nw}}{r} \right)^2, \quad (10)$$

and $\nu_t(x)$ the turbulent viscosity given by (Duguid et al. 2020):

$$\nu_t = v_c l_c F(\omega_t), \quad F(\omega_t) = \begin{cases} \frac{5}{2} (|\omega_t| t_c)^{-\frac{1}{2}} & |\omega_t| t_c < 10^{-2} \\ \frac{1}{2} (|\omega_t| t_c)^{-\frac{1}{2}} & |\omega_t| t_c \in [10^{-2}, 5] \\ \frac{25}{\sqrt{20}} (|\omega_t| t_c)^{-2} & |\omega_t| t_c > 5 \end{cases} \quad (11)$$

with v_c the convective velocity, l_c the mixing length, and t_c the convective turnover time.

2.3.2. Dynamical tide for progressive IGW

The dynamical tide is the tidal dissipation originating from the excitation of progressive gravity waves. These waves are excited with as frequency the tidal frequency ω_t . These IGW are dissipated through radiative damping, leading to the transfer of angular momentum between the stellar spin and its orbital motion.

Assuming the three layered structure (see Fig. 2), that can be reduced to a two layered structure, the tidal dissipation can

be calculated, for waves emerging from the convective core, and the convective envelope, as (Ahuir et al. 2021):

$$\begin{aligned} [\text{Im } k_2^2]_{\text{IGW}} = & \frac{3^{-\frac{1}{3}} \Gamma^2 \left(\frac{1}{3}\right)}{4\pi} m [l(l+1)]^{-\frac{4}{3}} \frac{\omega_t^{\frac{8}{3}}}{\Omega_o^4} \frac{GM_\star^2}{m_p^2 R_\star^5} \\ & \times \left(\rho_0(r_{\text{in}}) r_{\text{in}} \left| \frac{dN^2}{d \ln r} \right|_{r_{\text{in}}}^{-\frac{1}{3}} \mathcal{F}_{\text{in}}^2 \right. \\ & \left. + \rho_0(r_{\text{out}}) r_{\text{out}} \left| \frac{dN^2}{d \ln r} \right|_{r_{\text{out}}}^{-\frac{1}{3}} \mathcal{F}_{\text{out}}^2 \right) \end{aligned} \quad (12)$$

with m_p the mass of the planet, ρ_0 the unperturbed density at the inner and outer boundary of the radiative zone, \mathcal{F}_{out} and \mathcal{F}_{in} the tidal forcing term at the inner and outer boundary of the radiative zone, and Γ the gamma function. The tidal forcing term at the inner and outer boundary of the radiative zone can be expressed as (Ahuir et al. 2021):

$$\begin{aligned} \mathcal{F}_{\text{in}} &= \int_0^{r_{\text{in}}} \left[\left(\frac{r^2 \varphi_T}{g_0} \right)'' - \frac{l(l+1)}{r^2} \left(\frac{r^2 \varphi_T}{g_0} \right) \right] \frac{X_{1,\text{in}}}{X_{1,\text{in}}(r_{\text{in}})} dr, \\ \mathcal{F}_{\text{out}} &= \int_{r_{\text{out}}}^{R_\star} \left[\left(\frac{r^2 \varphi_T}{g_0} \right)'' - \frac{l(l+1)}{r^2} \left(\frac{r^2 \varphi_T}{g_0} \right) \right] \frac{X_{1,\text{out}}}{X_{1,\text{out}}(r_{\text{out}})} dr. \end{aligned} \quad (13)$$

where $X_{1,\text{out}}$ and $X_{1,\text{in}}$ are representations for the radial displacement originating from the inner and outer boundary of the radiative zone, and φ_T is the tidal potential. The radial displacement can be calculated using the following differential equations and boundary conditions (Ahuir et al. 2021):

$$\begin{cases} X_{1,\text{out}}'' - \frac{\partial_r \rho_0}{\rho_0} X_{1,\text{out}}' - \frac{l(l+1)}{r^2} X_{1,\text{out}} = 0 \\ X_{1,\text{out}}(r)_{r \rightarrow 0} \propto r^{1/2 + \sqrt{1/4 + l(l+1)}} \\ X_{1,\text{out}}'(r)_{r \rightarrow 0} \propto (1/2 + \sqrt{1/4 + l(l+1)}) r^{-1/2 + \sqrt{1/4 + l(l+1)}} \\ X_{1,\text{in}}'' - \frac{\partial_r \rho_0}{\rho_0} X_{1,\text{in}}' - \frac{l(l+1)}{r^2} X_{1,\text{in}} = 0 \\ X_{1,\text{in}}(r)_{r \rightarrow R_\star} \propto \rho_0 \left(r - R_\star - \frac{\varphi_T(R_\star)}{g_0(R_\star)} \right) \\ X_{1,\text{in}}'(r)_{r \rightarrow R_\star} \propto \rho_0(R_\star) \end{cases} \quad (14)$$

where the proportionality factor in the boundary conditions is irrelevant due as only $X/X(r_{\text{int}})$ is used. The boundary conditions are calculated by assuming $\frac{\partial_r \rho_0}{\rho_0}$ is small close to the center of the star, and $\frac{l(l+1)}{r^2}$ is small close to the surface of the star.

3. Stellar evolution models

To study the different tidal dissipation mechanisms throughout a stars lifetime, stellar evolutionary models are necessary. In this study we use the Modules for Experiments in Stellar Astrophysics (MESA) code (Paxton et al. 2011, 2013, 2015, 2018, 2019; Jermyn et al. 2023) to calculate these stellar evolutionary models. Models are computed for Zero Age Main Sequence (ZAMS) masses between 1 and $4 M_\odot$ at solar metallicity ($Z = 0.0134$; Asplund et al. 2009) for which the HR diagram is shown in Fig. 3¹.

¹ The inlist used to compute the stellar evolutionary models can be found on zenodo.

zenodo

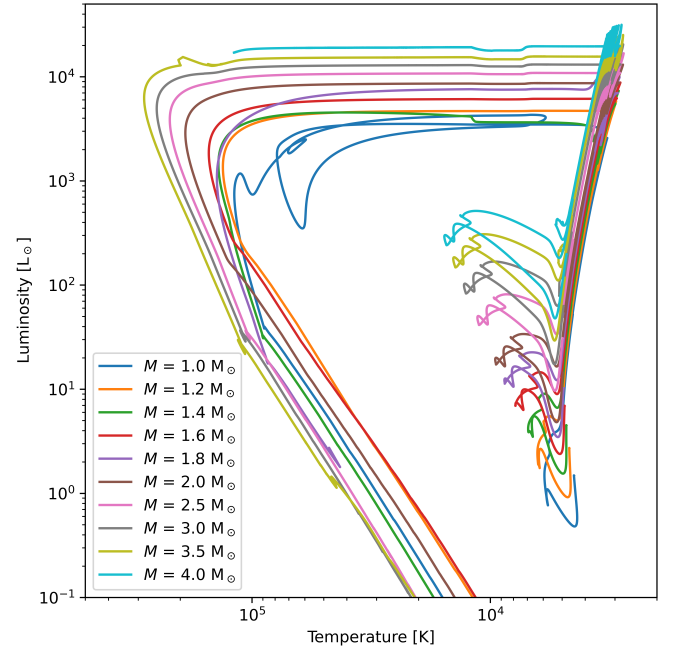


Fig. 3. HR diagram of the stellar evolutionary models computed with MESA.

update for recent models, $M = 4$ still running, $M = 1.8$ timestep error. Figures below is with different model

To simulate convection the Mixing Length Theory (MLT) is used, following the prescription of Henyey et al. (1965). In this prescription α_{MLT} is the mixing length parameter, which is calibrated by Cinquegrana & Joyce (2022) to reproduce the solar radius and luminosity at the solar age, resulting in $\alpha_{\text{MLT}} = 1.931$. Concerning the opacities in the star, as evolved stars have relative low temperatures, a dedicated low-temperature molecular opacity table AESOPUS (Marigo & Aringer 2009). For the atmosphere a grey $T - \tau$ relation is used, using the Eddington relation.

For mass-loss, the Reimers prescription (Reimers 1975) is used during the RGB phase, with $\eta_{\text{reimers}} = 0.477$ based on (McDonald & Zijlstra 2015). Later in the AGB phase, the Blöcker prescription (Blöcker 1995) is used, with $\eta_{\text{blöcker}} = 0.05$ for masses below $2 M_\odot$ and $\eta_{\text{blöcker}} = 0.1$ for masses above $2 M_\odot$ (Madappatt et al. 2016).

Stars undergo internal mixing, which is described by convective mixing in the convective zone, but in the radiative zone this is still under investigation. In this study a minimal amount of mixing was used, with a minimal diffusion coefficient of $D_{\text{min}} = 10^2 \text{ cm}^2 \text{ s}^{-1}$.

The models are terminated when the WD is cooled down sufficiently to produce a luminosity of $L = 10^{-1} L_\odot$.

4. Tidal dissipation along stellar evolution

During the evolution of the star, due to the changes in internal structure, tides are sometimes stronger and sometimes less strong. In this section we investigate the tidal dissipation along the stellar evolution.

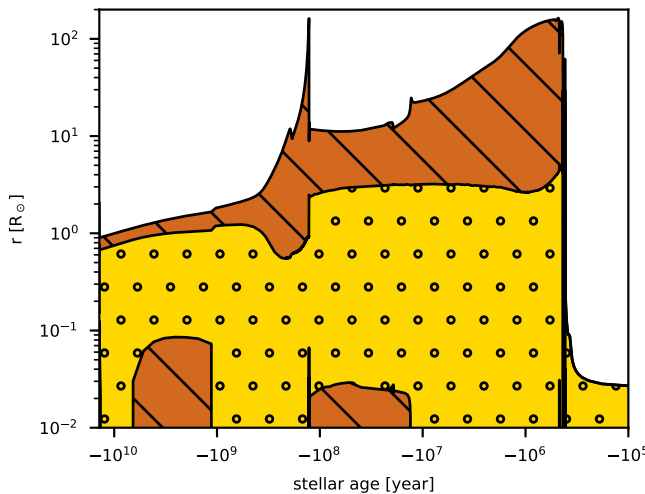


Fig. 4. Kippenhahn diagram for a $M_{\text{ZAMS}} = 1 \text{ M}_{\odot}$ star.

4.1. Earth around the sun

4.1.1. Internal structure of a 1 M_{\odot} star

First investigating the effect of tidal dissipation of a solar mass star. To start tidal dissipation depends strongly on the internal structure of the star, where the Kippenhahn of a $M_{\text{ZAMS}} = 1 \text{ M}_{\odot}$ star is shown. Here the stellar age is represented as time until the end of the simulation, thus time until the WD is cooled down to produce a luminosity of $L = 10^{-1} \text{ L}_{\odot}$. When plotting this time in logarithmic scale, the evolved phases can be shown in a single plot. The Kippenhahn diagram is shown in Fig. 4. The different phases are indicated in the figure. During the MS, the radius increases gradually, where the star has a convective envelope and a radiative core. During some part of the MS, the star also has a convective core, representing the three layered structure shown in Fig. 2. After the MS, the star starts to expand rapidly, the convective envelope grows, and the convective core disappears. During the RGB phase, the star has a convective envelope and a radiative interior. When the star reaches the tip of the RGB, the star contracts during the helium flash, where the radius of the star stays relative constant during the horizontal branch (HB). During this phase the star has a convective core again. After the HB, the star expands again, and the star has a convective envelope and a radiative interior again in the AGB phase. When the star reaches the tip of the AGB, the star contracts again, where the star leaves the AGB track to cool down as a WD. During the WD phase, the star has a radiative interior.

4.1.2. Tidal dissipation

Now assuming a planet with an orbit of 1 yr (e.g. the Earth), that is rotating around such a star (e.g. the Sun). For simplicity the orbit is assumed to remain at a period of 1 yr. When calculating the Love number for such a planet for both the equilibrium and dynamical tide along the evolution, Fig. 5 is obtained. Looking at the equilibrium tide, the Love number follows the trend of the radius quite well. When the radius increases, the Love number increases, and when the radius decreases, the Love number decreases. This is not the case for the dynamical tide. In the equations for the dynamical tide (Eq. 12) the Love number is proportional to R_{\star}^{-5} , and thus the dynamical tide responds inversely

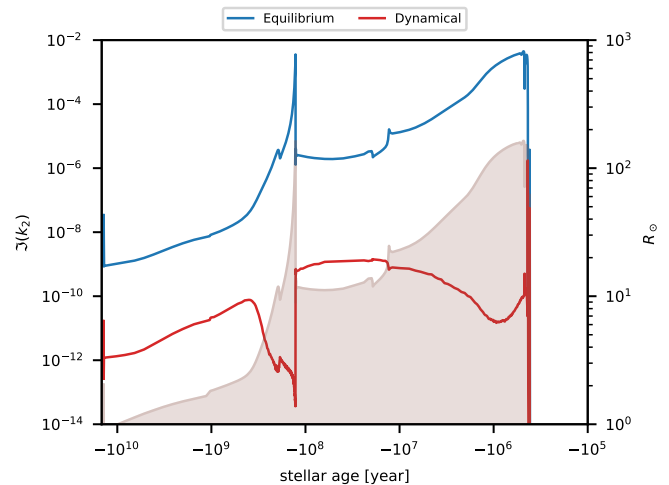


Fig. 5. Imk2 for Eq and Dyn as function of time, for a $M_{\text{ZAMS}} = 1 \text{ M}_{\odot}$ star.

to an increase in radius². This effect is compensated by the tidal forcing \mathcal{F} which includes some proportionality with R_{\star} as well. Multiplying their contributions, the tidal forcing wins and this component increases with stellar age. An other component that has a significant influence on the dynamical is the density at the interaction region. This density remains approximately constant during the MS, and reacts inversely to changes in radius. Therefore the Love number of the dynamical tide increases during the MS, decreases during the RGB, increases again to remain stable during the HB, and decreases during the AGB. During the WD phase, because the star has a negligible envelope, the tidal forcing decreases dramatically, so the dynamical tide is negligible during this phase.

Carefull, is our prescription valid for such systems of small/zero convective envelope during WD? See [Veras et al. 2019](#); [Veras & Fuller 2019](#)

Overall the tidal dissipation of the equilibrium tide here is dominant compared to the dynamical tide. But as they have different dependancies this will change for different orbital periods, as will be shown in the next section.

4.2. Dependance of tidal dissipation on orbital period

The strength of the equilibrium and dynamical tide are dependant on how far the planet is from the star. For the equilibrium tide this is captured in the linear dependance on ω_t , but there is also a complex dependancy in the turbulent viscosity. For the dynamical tide there is a dependancy in ω_t , n , the tidal forcing, and the boundary conditions of X . This results in a complex dependancy on orbital period which will be investigated here for a 1 M_{\odot} star.

4.2.1. Equilibrium tide

The equilibrium tide as a function of stellar age and orbital period are shown in Fig. 6. Here it can be seen that by increasing the orbital period, the equilibrium tide increases until a minimum is reached, and the equilibrium tide becomes weaker again.

² Note that this is for the Love number, when calculating the orbital evolution of the system, this factor of R_{\star}^5 cancels out.

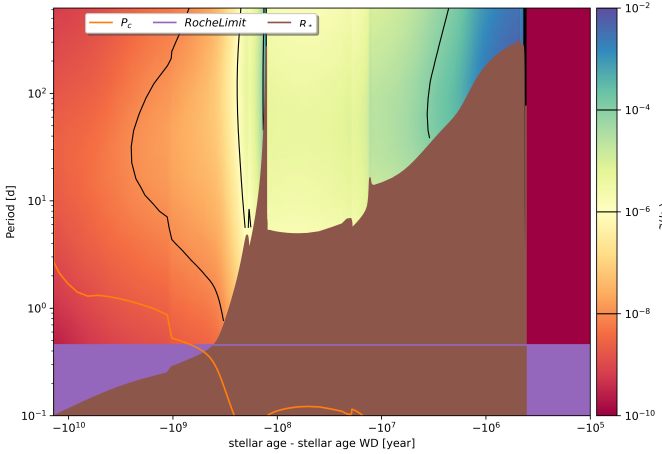


Fig. 6. Imk2 for Eq as function of orbital period, for a $M_{\text{ZAMS}} = 1 \text{ M}_{\odot}$ star.

This is because for low orbital period, the tidal frequency is sufficiently high such that in the dominant region the turbulent viscosity is proportional to the inverse square of the tidal frequency. Because there is an additional linear dependence on the tidal frequency in the Love number of the equilibrium tide, the equilibrium tide is proportional to the inverse of the tidal frequency, thus will increase with increasing orbital period. However, when the orbital period is sufficiently high, the tidal frequency is sufficiently low such that the turbulent viscosity is proportional to the inverse square root of the tidal frequency, and thus the equilibrium tide is proportional to the square root of the tidal frequency, and by increasing the orbital period further, the equilibrium tide will decrease again.

4.2.2. Dynamical tide

The dynamical tide as a function of stellar age and orbital period are shown in Fig. 7 (The white region is where the star has no convective region, thus no IGW can be formed, and there is no dynamical tide). Here it can be seen that by increasing the orbital period, the dynamical tide strictly decreases. Looking at Eq 12, there is a dependence in ω_t , n , the tidal forcing, and the boundary conditions of X . The tidal forcing is proportional to the inverse of the square of the orbital period (as there is a φ_T , which has a dependence of $a^3 \propto n^{-2}$), so this cancels out the direct dependence on the orbital frequency in the equation. The dependence in the boundary condition of X remains small, and only has a small effect at low orbital periods. The dependence on $\omega_t^{8/3}$ is the dominant factor, and thus the dynamical tide is proportional to the inverse of the orbital period to the power of 8/3.

4.2.3. Relative strengths

As the strengths of the equilibrium and dynamical tide have a different dependence on stellar age and orbital period, in some regions of the parameter space the equilibrium tide will be dominant, and in some regions the dynamical tide. This can be seen in Fig. 8, where the ratio of the equilibrium and dynamical tide is shown. During the MS, the dynamical tide is dominant for orbits lower than a few days, where there is a gradual change where the equilibrium tide dominates for orbits longer than 100 days. When the star enters the RGB, as the equilibrium tide increases in this phase, while the dynamical tide decreases, the equilib-

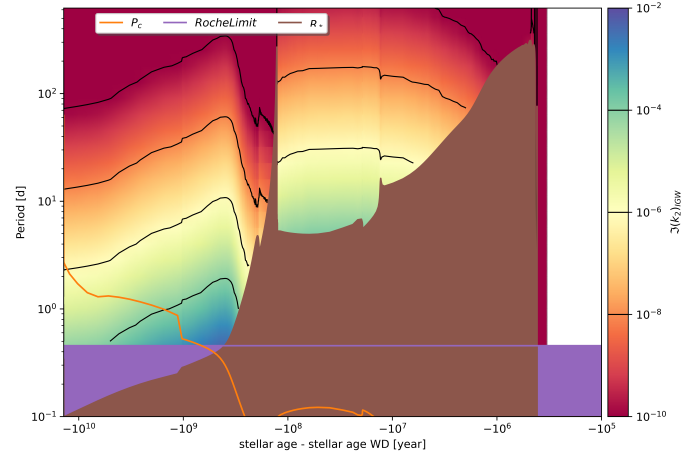


Fig. 7. Imk2 for Dyn as function of orbital period, for a $M_{\text{ZAMS}} = 1 \text{ M}_{\odot}$ star.

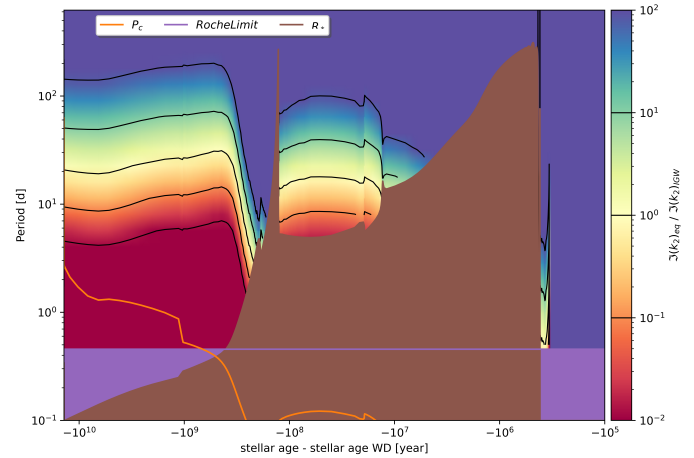


Fig. 8. Ratio of the Imk2 for Eq and Dyn as function of orbital period, for a $M_{\text{ZAMS}} = 1 \text{ M}_{\odot}$ star.

rium tide becomes dominant for shorter and shorter orbits, dominating completely when the star is sufficiently large. When the star contracts to the HB, the dynamical tide returns, having importance again for orbits up to a 100 days. When the star enters the AGB, the equilibrium tide becomes dominant again, similar to the RGB phase. When the star contracts to the WD, there is a short region where the dynamical tide has some importance, albeit small, but this stops abruptly as these models have no convective envelope, and thus no tidal forcing.

Should we be carefull with this?

4.3. Dependance of tidal dissipation on stellar mass

The strength of the equilibrium and dynamical tide are dependent on the mass of the star. In this section we investigate the dependence of the tidal dissipation on the stellar mass.

4.3.1. A $M_{\text{ZAMS}} = 1.4 \text{ M}_{\odot}$ star

First investigating the effect of tidal dissipation of a $M_{\text{ZAMS}} = 1.4 \text{ M}_{\odot}$ star. A Kippenhahn diagram is shown in Fig. 9, where the global trends are the same as for the $M_{\text{ZAMS}} = 1 \text{ M}_{\odot}$ star, but

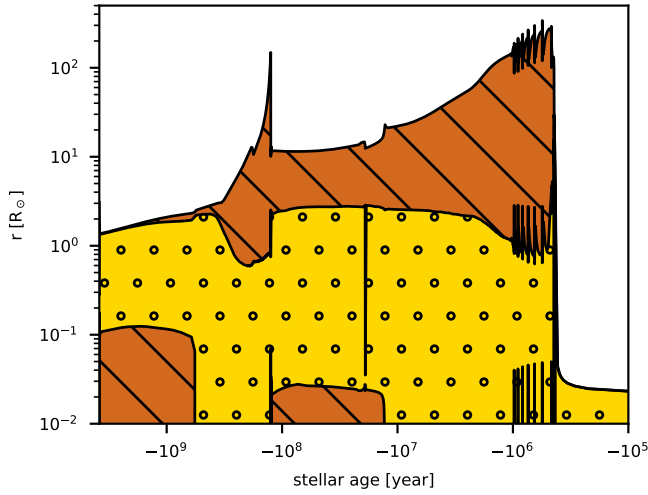


Fig. 9. Kippenhahn diagram for a $M_{\text{ZAMS}} = 1.4 \text{ M}_{\odot}$ star.

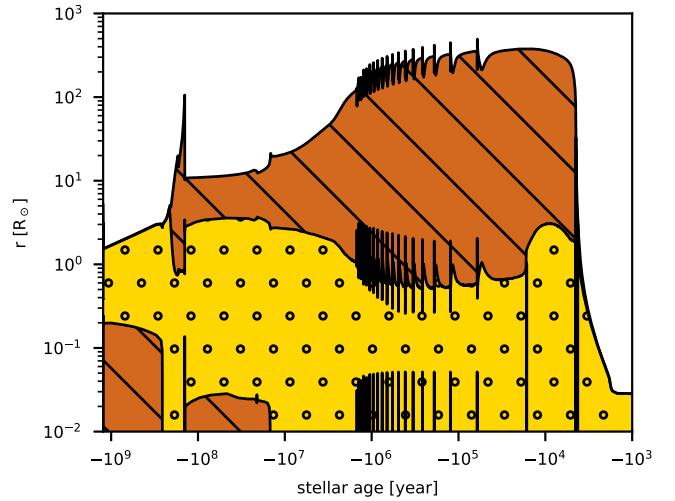


Fig. 11. Kippenhahn diagram for a $M_{\text{ZAMS}} = 2 \text{ M}_{\odot}$ star.

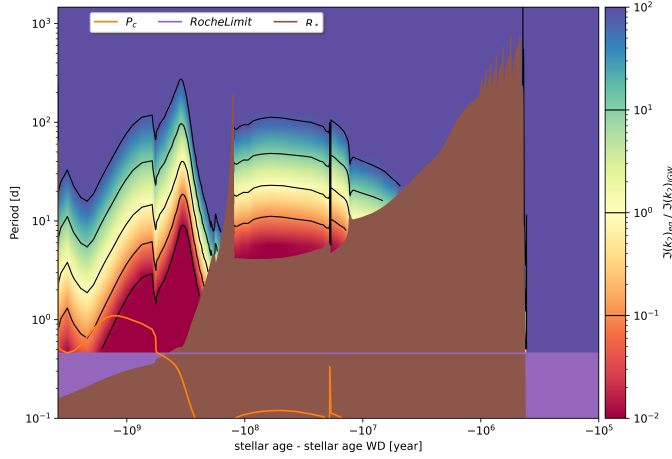


Fig. 10. Ratio of the Imk2 for Eq and Dyn as function of orbital period, for a $M_{\text{ZAMS}} = 1.4 \text{ M}_{\odot}$ star.

Fig. 9 and Fig. 10 can be combined, see Fig. B.2

in the MS, the convective envelope is significantly smaller. Because of this, both the equilibrium tide and the tidal component coming from the convective envelope become smaller, where the dynamical tide is effected the most, making the equilibrium tide more important in the MS. This can be seen in Fig. 10, where the ratio of the equilibrium and dynamical tide is shown for the $M_{\text{ZAMS}} = 1.4 \text{ M}_{\odot}$ star. When the star evolves during the MS, the convective envelope increases again, giving a more similar ratio as for the $M_{\text{ZAMS}} = 1 \text{ M}_{\odot}$ star. During the RGB, HB, AGB and WD phase, the ratio is similar to the $M_{\text{ZAMS}} = 1 \text{ M}_{\odot}$ star.

4.3.2. A $M_{\text{ZAMS}} = 2 \text{ M}_{\odot}$ star

Investigating the effect of tidal dissipation of a $M_{\text{ZAMS}} = 2 \text{ M}_{\odot}$ star. A Kippenhahn diagram is shown in Fig. 11, and the fraction of the Love numbers is given in Fig. 12. Here during the MS, the convective envelope is completely gone. For this reason the dynamical tide is dominated by the tidal forcing originating in the center of the star. During the MS, this component decreases as the radius of the interaction region decreases, while the radius

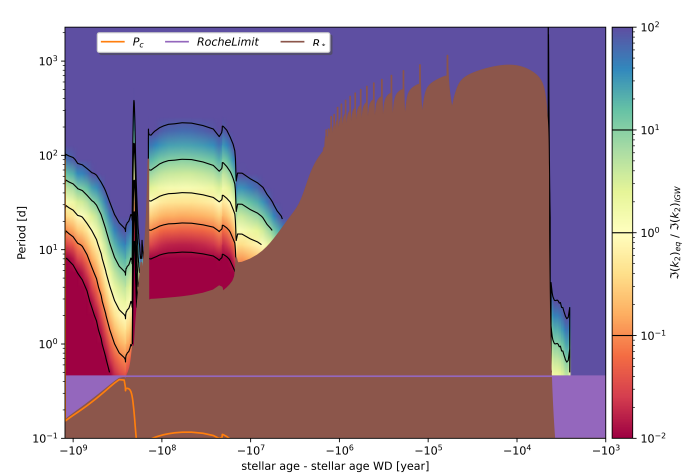


Fig. 12. Ratio of the Imk2 for Eq and Dyn as function of orbital period, for a $M_{\text{ZAMS}} = 2 \text{ M}_{\odot}$ star.

of the star increases again. From the moment the convective envelope reappears in the RGB, the importance of the dynamical tide shoots up again, while decreasing because of the increasing radius. During the HB, AGB and WD phase, the ratio is similar to the $M_{\text{ZAMS}} = 1 \text{ M}_{\odot}$ star, although notice that the region where the dynamical tide has some contribution now reaches above the tip of the RGB.

4.3.3. A $M_{\text{ZAMS}} = 3.5 \text{ M}_{\odot}$ star

Investigating the effect of tidal dissipation of a $M_{\text{ZAMS}} = 3.5 \text{ M}_{\odot}$ star. A Kippenhahn diagram is shown in Fig. 13, and the fraction of the Love numbers is given in Fig. 14. Just as in the $M_{\text{ZAMS}} = 2 \text{ M}_{\odot}$ star, the convective envelope is completely gone during the MS, where the dominance of the dynamical tide decreases because of the decreasing importance of the tidal forcing from the core. During the RGB, HB, AGB and WD phase, the ratio is similar to the $M_{\text{ZAMS}} = 2 \text{ M}_{\odot}$ star, where the region where the dynamical tide has some contribution reaches far above the top of the RGB, but still is below the tip of the AGB.

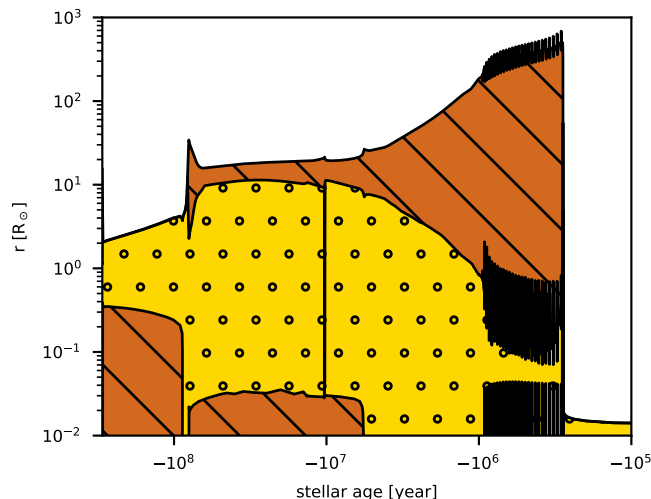


Fig. 13. Kippenhahn diagram for a $M_{\text{ZAMS}} = 3.5 \text{ M}_\odot$ star.

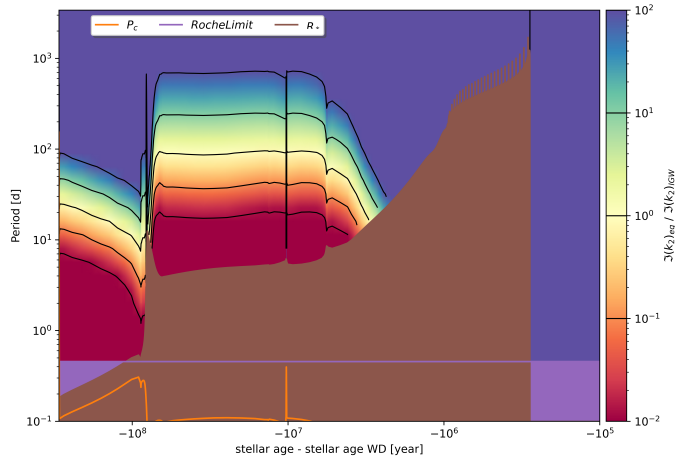


Fig. 14. Ratio of the Imk2 for Eq and Dyn as function of orbital period, for a $M_{\text{ZAMS}} = 3.5 \text{ M}_\odot$ star.

5. Conclusion

Conclusion

Acknowledgements. The authors would like to thank Matthias Fabry, Hannah Brinkman, and Pablo Marchant for their help and support in setting up the stellar evolution models. The authors would also like to thank Clément Baruteau for the usefull discussions.

[add funding](#)

References

- Ahuir, J., Mathis, S., & Amard, L. 2021, A&A, 651, A3
 Alvan, L., Strugarek, A., Brun, A. S., Mathis, S., & Garcia, R. A. 2015, A&A, 581, A112
 Asplund, M., Grevesse, N., Sauval, A. J., & Scott, P. 2009, ARA&A, 47, 481
 Auclair Desrotour, P., Mathis, S., & Le Poncin-Lafitte, C. 2015, A&A, 581, A118
 Barker, A. J. 2020, MNRAS, 498, 2270
 Blöcker, T. 1995, A&A, 297, 727
 Ceillier, T., Tayar, J., Mathur, S., et al. 2017, A&A, 605, A111
 Cinquegrana, G. C. & Joyce, M. 2022, Research Notes of the American Astronomical Society, 6, 77
 Dhouib, H., Baruteau, C., Mathis, S., et al. 2023, arXiv e-prints, arXiv:2311.03288

- Duguid, C. D., Barker, A. J., & Jones, C. A. 2020, MNRAS, 497, 3400
 García-Segura, G., Villaver, E., Langer, N., Yoon, S. C., & Manchado, A. 2014, ApJ, 783, 74
 García-Segura, G., Villaver, E., Manchado, A., Langer, N., & Yoon, S. C. 2016, ApJ, 823, 142
 Henyey, L., Vardya, M. S., & Bodenheimer, P. 1965, ApJ, 142, 841
 Jermyn, A. S., Bauer, E. B., Schwab, J., et al. 2023, ApJS, 265, 15
 Madappatt, N., De Marco, O., & Villaver, E. 2016, MNRAS, 463, 1040
 Marigo, P. & Aringer, B. 2009, A&A, 508, 1539
 McDonald, I. & Zijlstra, A. A. 2015, MNRAS, 448, 502
 Mustill, A. J. & Villaver, E. 2012, ApJ, 761, 121
 Ogilvie, G. I. 2013, MNRAS, 429, 613
 Ogilvie, G. I. 2014, ARA&A, 52, 171
 Paxton, B., Bildsten, L., Dotter, A., et al. 2011, ApJS, 192, 3
 Paxton, B., Cantiello, M., Arras, P., et al. 2013, ApJS, 208, 4
 Paxton, B., Marchant, P., Schwab, J., et al. 2015, ApJS, 220, 15
 Paxton, B., Schwab, J., Bauer, E. B., et al. 2018, ApJS, 234, 34
 Paxton, B., Smolec, R., Schwab, J., et al. 2019, ApJS, 243, 10
 Reimers, D. 1975, in *Problems in stellar atmospheres and envelopes.*, 229–256
 Veras, D., Efroimsky, M., Makarov, V. V., et al. 2019, MNRAS, 486, 3831
 Veras, D. & Fuller, J. 2019, MNRAS, 489, 2941
 Weinberg, N. N., Sun, M., Arras, P., & Essick, R. 2017, ApJ, 849, L11
 Wu, Y. 2005a, ApJ, 635, 674
 Wu, Y. 2005b, ApJ, 635, 688

Appendix A: Comparison to (Ahuir et al. 2021) for MS and PMS

Appendix B: Alternative figures for Kipp diagram, and Imk2 ratio

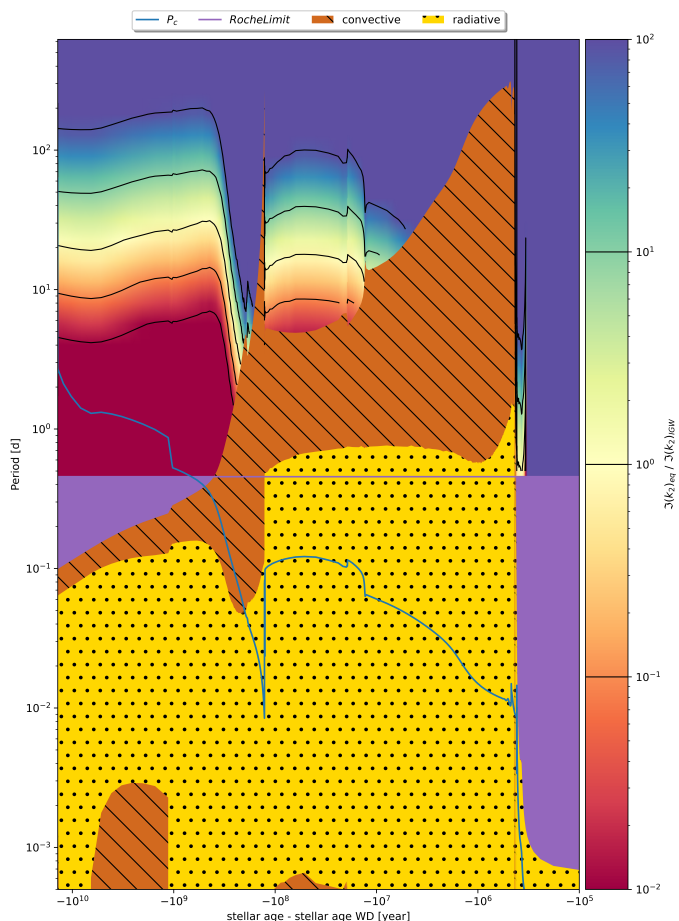


Fig. B.1. Kippenhahn diagram and Imk2 ratio for a $M_{\text{ZAMS}} = 1 \text{ M}_{\odot}$ star.

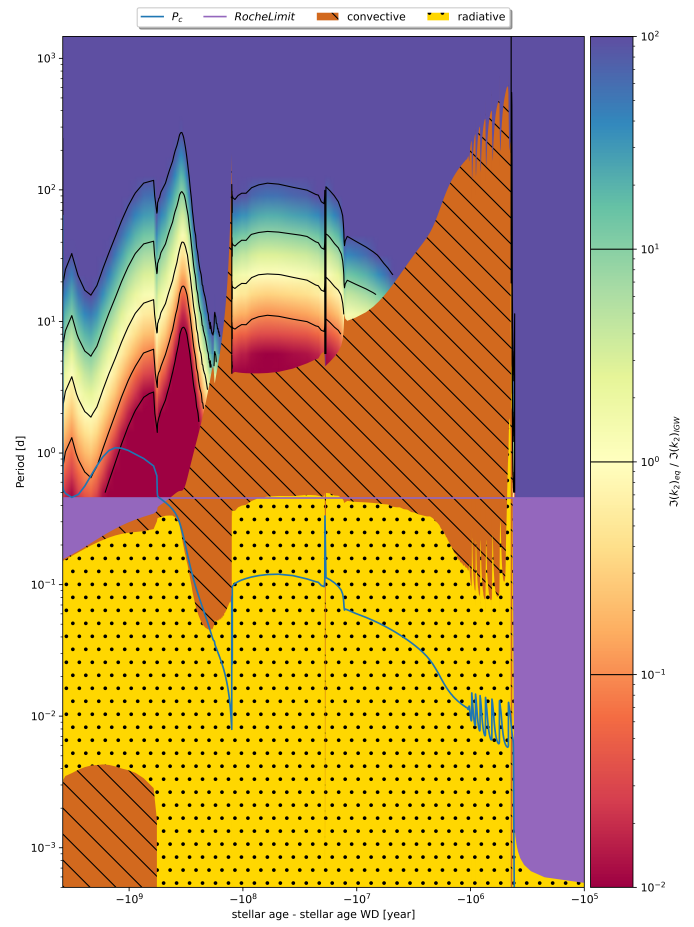


Fig. B.2. Kippenhahn diagram and Imk2 ratio for a $M_{\text{ZAMS}} = 1.4 \text{ M}_{\odot}$ star.